ACS APPLIED MATERIALS & INTERFACES

www.acsami.org

Research Article

Tuning of Ultra-Thin Gold Films by Photoreduction

Daniel Martínez-Cercós,* Bruno Paulillo, Jessica Barrantes, Jose Mendoza-Carreño, Agustín Mihi, Todd St. Clair, Prantik Mazumder, and Valerio Pruneri*

Cite This: *ACS Appl. Mater. Interfaces* 2023, 15, 16204−16210

Read Online

ACCESS | Metrics & More | Article Recommendations | Supporting Information

ABSTRACT: Ultrathin metal films (UTMFs) are used in a wide range of applications, from transparent electrodes to infrared mirrors and metasurfaces. Due to their small thickness (<5 nm), the electrical and optical properties of UTMFs can be changed by external stimuli, for example, by applying an electric field through an ion gel. It is also known that oxidized thin films and nanostructures of Au can be reduced by irradiating with short-wavelength light. Here we show that the resistance, reflectance, and resonant optical response of Au UTMFs is changed significantly by ultraviolet light. More specifically, photoreduction and oxidation processes can be sequentially applied for continuous tuning, with observed modulation ranges for sheet resistance (*Rs*) and reflectance of more than 40% and 30%, respectively. The proposed method has the potential for achieving reconfigurable UTMF structures and trimming their response to specific working points, e.g., a predetermined resonance wavelength and amplitude. This is also important for large scale deployment of such surfaces as one can compensate material nonuniformity, morphological, and structural dimension errors occurring during fabrication.

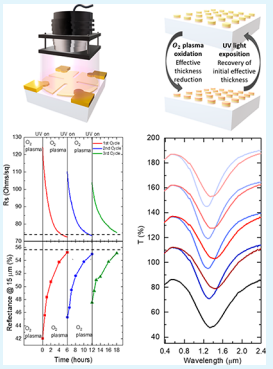

KEYWORDS: *ultrathin, gold, auric oxide, redox, ultraviolet, photoreduction, plasmonics*

INTRODUCTION

In recent years, ultrathin metal films (UTMFs) have garnered high interest in many applications such as transparent conductors,[1,2] infrared optics,[3] and plasmonic metasurfaces[4,5] to name a few. UTMF nanostructures can be tailored to achieve application-specific electrical and optical properties, for example through choice of metals and/or geometrical parameters. However, the control of these parameters in order to achieve the desired device performance can go beyond small-scale fabrication technology capabilities, especially when low cost and large-scale fabrication techniques are used. One solution is postfabrication tuning that can also provide device reconfigurability. In this regard, thanks to their thinness, the optical response of UTMFs can be electrically tuned using ion gels.[4,6] It has also been shown that the electrical transport properties of thin metals can change depending on reduction or oxidation reactions occurring on the surface.[7]

Several papers have reported the formation of gold oxide (Au_2O_3) on UTMFs and nanoparticles of Au in processes such as pulsed laser deposition (PLD) and sputtering in an oxygen atmosphere,[8,9] or after exposure to highly reactive chemical environments such as ozone,[10] high frequency activated O_2[11] or dc-glow discharge oxygen plasma.[12] This oxidation occurs despite the fact that the heat of formation is estimated to be around +19.3 kJ/mol.[13] So far, there is no consensus on the origin of formation of the superficial AuO_x layer, as its thickness, chemical composition, stability, and the coexistence of different oxygen species are dependent on the oxidation method and on gold morphology (size and shape).[14,15] Reported values of AuO_x layer thicknesses range from 0.5 to a few nanometers, which decompose to its metallic state (Au^0) in ambient conditions after some days.[14,16] It has also been shown that the reduction process can be shortened to a few hours by applying UV irradiation.[12] The formation or reduction of nanometer or less superficial oxide layers is not expected to significantly change the optical and electrical properties of metallic structures with geometrical features in the range of tens or hundreds of nanometers, such as metallic thin films, clusters, or particles. However, it is expected to greatly affect electrical and optical properties of UTMFs due to their thinness (below 10 nm).

In this paper, we demonstrate that photons can induce significant changes in the electrical and optical properties of Au UTMFs. More specifically, we show that oxidation and photoreduction processes can be sequentially applied for continuous tuning of electrical resistance and optical reflectivity of uniform UTMFs as well as the resonant plasmonic response of nanopatterned structures. The observed modulation ranges for the sheet resistance (*Rs*) and the reflectance reached large values, more than 40% and 30%, respectively. The shorter the wavelength and the thinner the UTMF, the larger the tuning effect due to photoreduction. On the one hand, this light tuning offers a unique capability for

Received: December 8, 2022
Accepted: March 12, 2023
Published: March 20, 2023

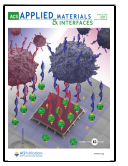

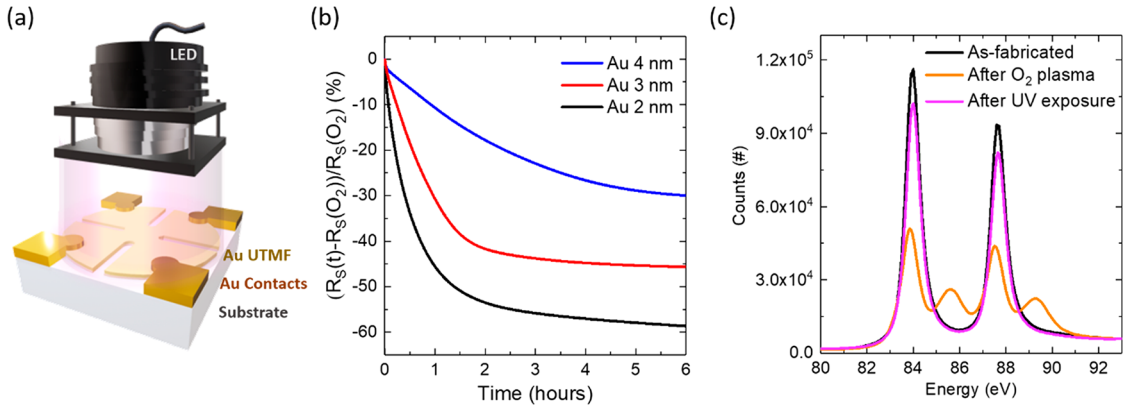

Figure 1. O_2 plasma-oxidized Au UTMFs under ultraviolet (UV) irradiation: light wavelength (λ) is 365 nm, intensity (I) is ~100 mW/cm^2. The controlled environment is at a temperature (T) of 25 °C and a relative humidity (RH) of 60%. (a) Schematics of the experiment. (b) Evolution of the relative sheet resistance (R_S) with UV irradiation of previously O_2 plasma exposed Au UTMFs with mass-equivalent thicknesses of 4, 3, and 2 nm, respectively. Samples R_S values before and after O_2 plasma exposure are R_S(i) = 34.2, 75.8, and 274.7 Ω/sq and $R_S(O_2)$ = 46.8, 135.6, and 862.2 Ω/sq, respectively. (c) Au 4f scans using X-ray photoelectron spectroscopy (XPS) of a Au 3 nm UTMF after fabrication (black), after exposition to O_2 plasma (orange), and after UV irradiation (purple) for ~20 h. Characteristic Au 4f XPS peak doublets corresponding to the oxidation states Au^0 at 84.0 and 87.7 eV (ΔE = 3.7 eV) for the after fabrication and after UV irradiation cases, and Au^0 at 83.9 and 87.5 eV and Au^{3+} at 85.6 and 89.3 eV for the after O_2 plasma exposure case, can be identified.[17]

surface tailoring. On the other hand, our study reveals a method for trimming the response of UTMFs and related nanostructures to specific working points, e.g., a predetermined resonance frequency and amplitude, thus compensating for material nonuniformity, and morphological and structural dimensional variability occurring during fabrication.

RESULTS AND DISCUSSION

Figure 1a shows the experimental setup for measuring the sheet resistance of 0.5 nm CuO-seeded Au UTMFs (see details in Methods) on high-purity fused silica (HPFS) substrates under ultraviolet (UV) irradiation emitted by a light emitting diode (LED). The UTMFs were patterned in a cloverleaf shape and Ti/Au contacts were fabricated to precisely measure the resistivity by the 4-probe Van der Pauw method (see details in Methods). All the measurements were performed inside a well-controlled climate chamber at temperature T = 25 °C and relative humidity RH = 60%. For the experiments, 0.5 nm CuO-seeded Au UTMFs with nominal (mass equivalent) thickness, t, above or equal 2 nm were used. In our previous work,[6] it was demonstrated that the use of a 0.5 nm CuO seed layer promotes early percolation and continuity of the Au UTMFs. The CuO-seeded Au UTMFs percolate at t < 1.2 nm and show negligible porosity at t = 3 nm. First, when Au UTMFs of thicknesses 4, 3, and 2 nm with a certain initial sheet resistance, R_S(i), are exposed to O_2 plasma (see details in Methods), we observe that the films' resistance shifts to higher values, $R_S(O_2)$. This higher resistance can be reduced again to final values, R_S(f), approaching R_S(i), by UV light irradiation, as illustrated in Figure 1b, which shows the *in situ* relative $R_S(t)$ as a function of time of previously O_2 plasma-oxidized Au UTMFs, $\frac{R_S(t) - R_S(O_2)}{R_S(O_2)}$, for different mass-equivalent thicknesses under UV (λ = 365 nm) light with irradiation I ~ 100 mW/cm^2. Representative samples R_S before and after O_2 plasma values are R_S(i) = 34.2, 75.8, and 274.7 Ω/sq and $R_S(O_2)$ = 46.8, 135.6, and 862.2 Ω/sq, for the different thicknesses, respectively. When illuminated with UV light, a thickness-dependent decrease in the sheet resistance of the film with respect to its value after O_2 plasma exposure is observed. As the film thickness decreases, the relative change increases. The final sheet resistance values after 6 h of UV irradiance are R_S(f) = 32.7, 73.5, and 353.3 Ω/sq respectively, giving a total relative change, $\frac{R_S(f) - R_S(O_2)}{R_S(O_2)}$, of about −30, −46 and −59% for the Au 4, 3, and 2 nm UTMFs, respectively. In the case of the 4 and 3 nm thick Au UTMFs, the final sheet resistances are slightly below their values before O_2 plasma exposure. This effect is consistent with an initial oxidation state of the sample surface different than the pure metallic Au^0. Therefore, results indicate a recovery of the O_2 plasma exposed Au 4 and 3 nm thick UTMF samples close to their initial state. In the case of the 2 nm Au UTMF, R_S after UV irradiation is about 30% higher than its initial value before O_2 plasma exposure, which could be explained by sample degradation during the process due to nonrecovered parts to their initial state or morphological restructuring of the UTMF.[9] This effect may be more noticeable in Au 2 nm UTMFs since they present a higher film porosity than thicker films, as observed in previous work.[6] Figure 1c shows Au 4f scans using X-ray photoelectron spectroscopy (XPS) on a nonpatterned Au UTMF with mass equivalent thickness t = 3 nm on an HPFS substrate at three different stages of the process: as-fabricated, after O_2 plasma exposure, and after UV (λ = 365 nm) irradiation for ~20 h. In the XPS spectra of the as-fabricated sample, the Au($4f_{7/2}$) and Au($4f_{5/2}$) core level binding energies are centered at 84.0 and 87.7 eV (ΔE = 3.7 eV), respectively, which are in good agreement with the known binding energy of pure metallic Au^0.[17] After O_2 plasma exposure, two sets of peaks can be observed with maxima at 83.9 and 87.5 eV, and 85.6 and 89.3 eV, corresponding to the Au oxidation states Au^0 and Au^{3+} indicating metallic Au and AuO_x formation, respectively.[17] The AuO_x composition can be identified from O 1s scans using XPS on the 3 nm Au UTMF after O_2 plasma exposition (see SI, Figure S1). Two main binding energy peaks, which can be associated with oxygen in Au_2O_3 and $Au(OH)_3$ forms, can be observed. These results indicate that there might be different possible oxidation pathways via Au surface interaction with oxygen species and/or hydroxyl radicals, present before or generated by exposure to O_2 plasma.[18] After UV exposure

https://doi.org/10.1021/acsami.2c22149
ACS Appl. Mater. Interfaces 2023, 15, 16204−16210

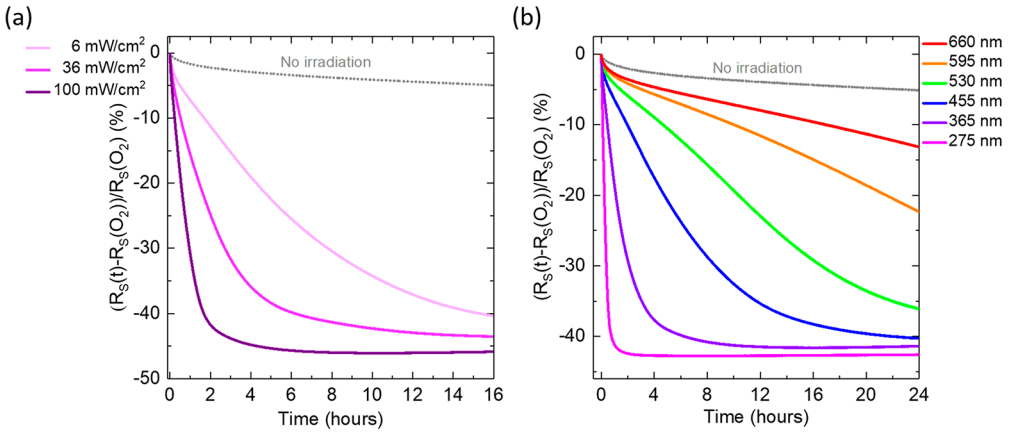

Figure 2. Characterization of the light induced (accelerated) AuO_x reduction process at controlled environment T = 25 °C and RH = 60%, of previously O_2 plasma exposed Au 3 nm UTMF. (a) Relative R_S evolution up to 16 h of exposure under UV (λ = 365 nm) LED light at different intensity levels, ∼100, 36, and 6 mW/cm^2, and no irradiation. Samples R_S before and after O_2 plasma values are R_S(i) = 75.8, 75.1, 76.4, and 77.3 Ω/sq and $R_S(O_2)$ = 135.6, 131.8, 138.5, and 146.9 Ω/sq respectively, for the different intensities and no irradiation case, respectively. (b) Relative R_S change evolution under irradiation with different LED light wavelengths, λ = 275, 365, 455, 530, 595, and 660 nm up to 24 h of exposure and all at the same intensity of ∼50 mW/cm^2. Samples R_S before and after O_2 plasma values are R_S(i) = 64.3, 62.1, 64.8, 62.8, 65.2, and 61.5 Ω/sq and $R_S(O_2)$ = 101.3, 100.3, 105.1, 103.6, 108.3, and 102.9 Ω/sq, for the different LED wavelengths used, respectively.

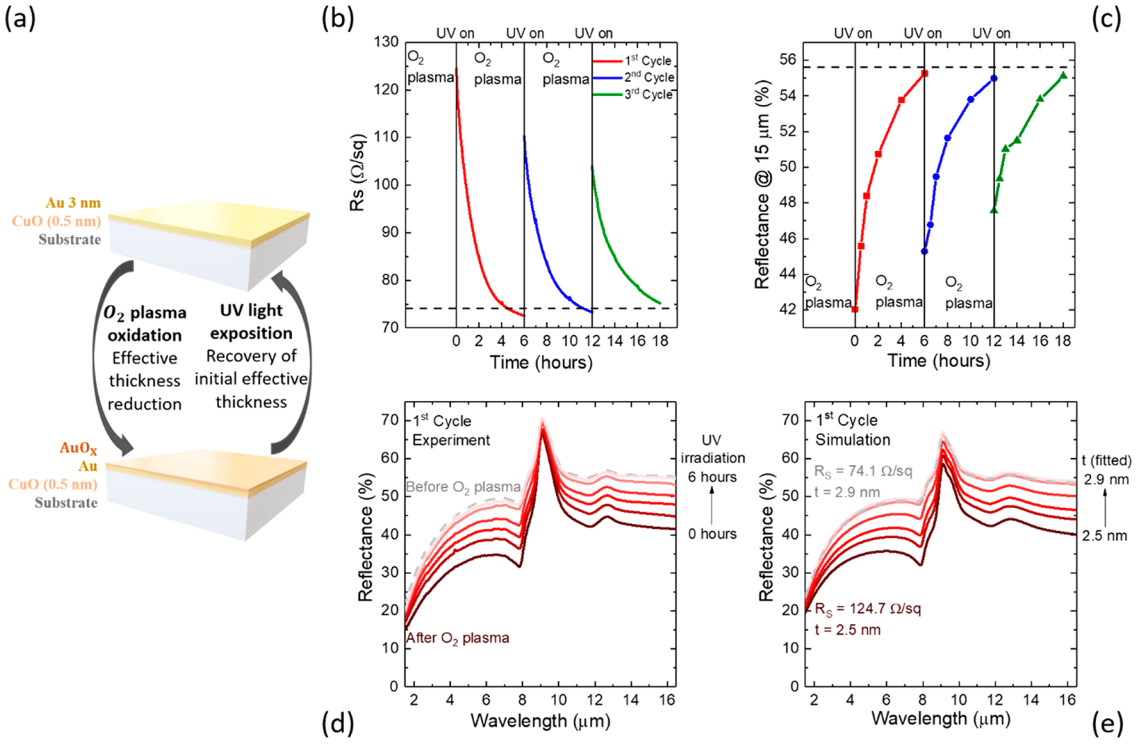

Figure 3. Tuning of electrical and optical properties by O_2 plasma oxidation and UV (λ = 365 nm) light irradiation in controlled atmosphere (T = 25 °C and RH = 60%) (a) Conceptual view of reconfigurable surface with Au UTMF of nominal (mass-equivalent) thickness (t) of 3 nm. (b) Sheet resistance R_S and (c) infrared (IR) reflectance at 15 μm during three cycles of O_2 plasma and UV irradiation, with dashed lines indicating initial values of the film (before O_2 plasma). (d) Measured and (e) simulated from the R_S values IR reflectance of the Au UTMF during the first cycle.

there is almost complete recovery of the sample to the initial state apart from some small residual signal at the Au^{3+} binding energies. The R_S evolution curves under UV irradiation together with the XPS study indicate that when the Au UTMFs are exposed to O_2 plasma, a superficial layer of AuO_x is formed which can be reduced by UV irradiation. These results are in agreement with previous studies.[12]

In order to further characterize this effect, we studied the light intensity and wavelength dependence of the photo-reduction process. Figure 2a shows the relative change in Rs with time after plasma oxidation and under UV (λ = 365 nm) illumination with three different intensity (I) levels of ∼100, 36, and 6 mW/cm^2. The data were collected from 4 different Au UTMFs (3 nm) from the same fabricated batch (with similar initial R_S). When no light is applied (curve labeled "No irradiation"), there is a very slow decomposition of the oxide layer reaching a relative change of around −11% after 3 days (see SI, Figure S2). This effect is significantly accelerated as we

https://doi.org/10.1021/acsami.2c22149
ACS Appl. Mater. Interfaces 2023, 15, 16204−16210

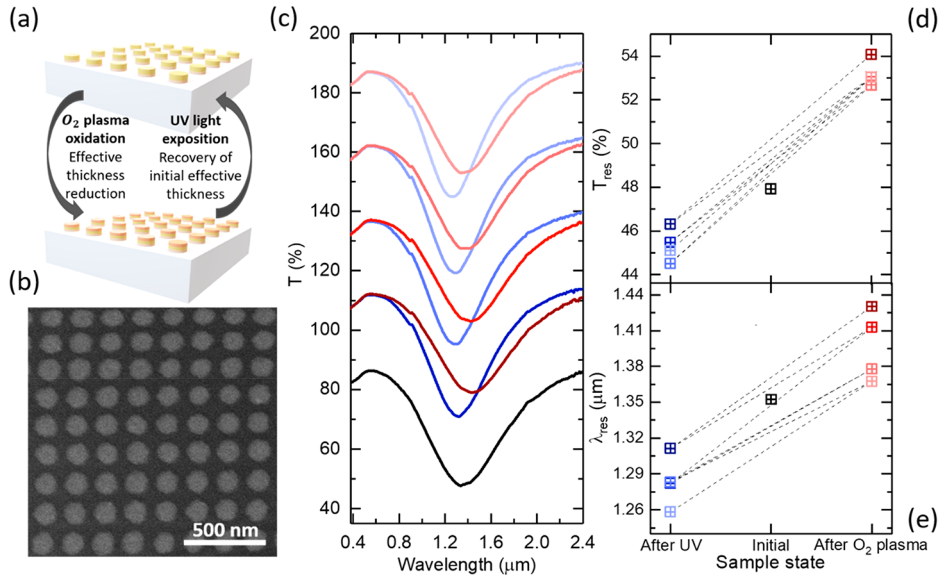

Figure 4. Reconfigurable plasmonic resonant metasurface. (a) Conceptual view of the plasmonic structure and tuning based on oxidation and photoreduction of Au UTMFs. (b) SEM image of the nanodisks patterned from a 4 nm Au UTMF. (c) Visible (VIS) and near IR (NIR) transmittance optical spectra of nanodisks as-fabricated (black), after O_2 plasma oxidation (red) and after UV photoreduction process (blue). The as-fabricated spectrum is shown in real scale; meanwhile, a 25%, 50%, 75%, and 100% offset in transmittance has been added to the first, second, third, and fourth oxidation and photoreduction cycles, respectively. (d, e) Transmittance and wavelength values at the minimum of the resonance depth of the nanodisks UTMF metasurface as-fabricated (black), after O_2 plasma oxidation (red), and after the UV photoreduction process (blue).

start illuminating the sample with UV light (λ = 365 nm) showing a clear dependence of the speed of the process with respect to the UV power, with a faster recovery of the sample R_S to its initial state as the power is increased. Figure 2b shows the relative change in R_S with time after plasma oxidation and under irradiation with LED light of different wavelengths and same intensity (~50 mW/cm^2). The data was collected from 7 different Au UTMFs (3 nm) from the same fabricated batch (with similar initial R_S). In comparison with the "No irradiation" case, the photoreduction acceleration occurs for all the tested wavelengths in the UV/vis range (from 275 to 660 nm) and is faster for shorter wavelengths, in agreement with what has been reported for thicker films.[12] Previous studies have attributed the UV induced reduction of metal oxides to different mechanisms. On the one hand, Higo et al.[12] speculate that vibrationally excited water molecules and/or hydrogen atoms and hydroxyl radicals, produced by UV photochemical splitting of water molecules, may interact with the surface of plasma oxidized gold films, contributing to their reduction to its metallic state. On the other hand, Fleisch et al.[19] proposed a model to explain the UV-induced reduction of metal oxide films. This model postulates that absorption of light by a metal oxide semiconductor can excite electrons from states near the top of the valence band into the conduction band of the solid, where if a vacant metal ion orbital is available when the photoexcited electron is thermalized, i.e., de-excited, the capture of the photoexcited electron by the metal ion is possible and results in its reduction. As for the origin of the photoreduction of oxidized ultrathin Au films observed in our experiments and whether previously proposed mechanisms can explain our observations, this would require extensive studies that go beyond the scope of this paper but will be considered in the future.

Following the observation that a combination of O_2 plasma oxidation and UV irradiation allows tuning of the electrical and optical response of Au UTMFs, we have prepared samples to demonstrate reconfigurable surfaces. More specifically, the samples we prepared are an electrically conductive and IR reflective surface (IR mirror, Figure 3) and a near IR plasmonic surface (resonant metasurface, Figure 4). Both structures underwent several cycles of O_2 plasma oxidation followed by UV photoreduction.

Figure 3a shows the conceptual view of the reconfigurability process based on O_2 plasma oxidation followed by UV photoreduction method. Figure 3a and b shows the sheet resistance and IR reflection evolution during the reconfiguration process of a 0.5 nm CuO-seeded 3 nm Au UTMF on high purity fused silica (HPFS) substrate. The Au UTMF after fabrication had a sheet resistance, R_S(i), and a reflectance at 15 μm, $R_{15\ \mu m}$(i), of 74.1 Ω/sq and 55.6%, respectively. After plasma oxidation, these values became $R_S(O_2)$ = 124.7 Ω/sq and $R_{15\ \mu m}(O_2)$ = 42.0%, respectively. After UV irradiation, the oxidized Au UTMF surface is slowly reduced to its metallic state reaching R_S(f) = 72.6 Ω/sq and $R_{15\ \mu m}$(f) = 55.3%, both close to the initial values. Two additional oxidation and photoreduction cycles were applied, and similar behavior was observed with a reduced range of modulation. The reduction of the effect with number of cycles could be attributed to cumulative changes of either or both chemical surface state[10] and morphology[9] of the sample when it undergoes oxidation and reduction processes. Figure 3d shows experimental IR spectra from 1.5 to 16.5 μm of the Au 3 nm UTMF of the first oxidation and reduction cycle at different times. In our previous work,[6] it was shown that, above percolation, the experimental optical response for the CuO-seeded Au UTMFs can be modeled as that of a homogeneous conductive film with same t with a Drude permittivity and an electron scattering time properly adjusted. Therefore, by calculating the Drude scattering time (τ) from experimental R_S values and interpolating the UTMF thickness (t) from the 0.5 nm CuO-seeded Au UTMF percolation curve,[6] we can simulate the experimental IR reflectance tuning by changing t and τ (see

https://doi.org/10.1021/acsami.2c22149
ACS Appl. Mater. Interfaces 2023, 15, 16204−16210

details in Methods). Figure 3e shows the simulated reflectance spectra of Au UTMFs with calculated τ and fitted t values from experimental R_S data of the sample measured during the first cycle. From the simulations, we can observe that the reflectance modulation range corresponds to a change in nominal (mass-equivalent) Au UTMF thickness from 2.5 to 2.9 nm. Note that this does not necessarily mean that the 3 nm Au UTMF film after O_2 plasma has the same morphology as that of an as-deposited film with a mass-equivalent thickness of 2.5 nm, but rather they have equivalent electrical and optical behavior. The reflectance data in this experiment are normalized with respect to a nearly fully reflective thick (50 nm) Au film deposited on the same substrate close the measured sample region. The peak in reflectivity observed at about 10 μm, in both experimental and simulated data, is associated with the fused silica substrate's Reststrhalen band.[20]

Figure 4a and b shows the representation and scanning electron microscopy (SEM) picture of a plasmonic metasurface consisting of a 4 nm Au UTMF patterned in an ordered nanodisk array (with diameter d = 115 nm and period p = 200 nm), respectively. The 1 cm^2 patterned area was obtained through a scalable fabrication method consisting of nano-imprinted holes on PMMA over a HPFS substrate, followed by 0.5 CuO-seeded 4 nm Au 4UTMF deposition and lift-off (see details in Methods). Figure 4c shows the transmittance spectra of the as-fabricated plasmonic metasurface and after 4 consecutive oxidation and UV accelerated reduction cycles. Measurements were performed right after O_2 plasma exposure and after 1 day of UV irradiation in order to achieve full reduction of the film. Note that, for data representation in Figure 4c, the as-fabricated spectrum is shown in real scale meanwhile a 25%, 50%, 75%, and 100% offset in transmittance has been added to the first, second, third, and fourth oxidation and photoreduction cycles, respectively. The as-fabricated sample shows an initial resonance depth in transmittance with minimum of T_{res} = 47.93% μm at λ_{res} = 1.35 μm. After O_2 plasma exposure, the nanodisk resonance loses strength and its minimum is red-shifted to $T_{res\_O_2}$ = 54.08% at $\lambda_{res\_O_2}$ = 1.43 μm. These changes are attributed to an effective reduction of the UTMF thickness due to surface oxidation that causes a change in the effective electrical conductivity (see refs 4 and 6), which in turn changes the resonance wavelength and strength. Thus, exposing the sample to UV radiation we are able to blue-shift and increase the strength of the resonance with a new minimum of T_{res_UV} = 46.32% at λ_{res_UV} = 1.31 μm. This change corresponds to a relative change with respect to the oxidized state of −14.3% and −8.3% for the transmittance and wavelength of the resonance minimum, respectively. This effect is due to the recovery of the UTMF to its metallic state, increasing its effective metallic thickness. During the next consecutive 3 cycles, the same behavior can be observed but with a continuous shift to shorter wavelengths and deeper resonance minimum, as shown in Figures 4d and e. This change might be associated with border effects, meaning an incomplete recovery or degradation of the edges of the structure, making it smaller every time the sample is cycled.[5]

CONCLUSIONS

We have shown that the electrical and optical properties of Au UTMFs can be reversibly tuned after fabrication via O_2 plasma oxidation and subsequent UV photoreduction processes which, as expected, decreases and increases the effective metallic thickness of the film, respectively. We demonstrated that the large conductivity modulation associated with the low thickness of the oxidized/photoreduced films can be exploited to reconfigure the response of UTMF-based optical surfaces, for example, as planar reflectors and near-IR plasmonic metasurfaces.

METHODS

UTMF Fabrication. Before growth, the substrates (UV-grade high purity fused silica from Corning Inc.) were cleaned with acetone in a ultrasonic bath followed by rinsing in isopropanol (5 min for each process) and drying under a nitrogen flow. Then, the substrates were exposed to an O_2 plasma with an oxygen flow of 200 mL/min and power of 150 W for 3 min, in a plasma asher (Tepla 300). For the CuO seed deposition the substrates were introduced in the sputtering chamber that is evacuated to a base pressure of about 10^{-7}−10^{-8} Torr. A cupric oxide (CuO) sputtering target of 99.7% purity was used for seed layer deposition with a RF power of 150 W and working pressure of 2 mTorr in an argon and oxygen atmosphere (20 and 2 sccm respectively). Oxygen was added to compensate for the possible reduction of the CuO during sputtering. The extrapolated deposition rate is 0.2 Å/s, which corresponds to a 24 s deposition time for 0.5 nm CuO. During the CuO seed deposition, the substrate holder was rotating at a speed of 60 rpm. Au UTMFs were deposited via thermal evaporation in a separate vacuum chamber, previously evacuated to a base pressure of about 10^{-7}−10^{-8} Torr, where the substrates are immediately transferred after CuO seed preparation. The Au thermal evaporation rate is 1 Å/s *in situ* measured by a quartz crystal microbalance. In the case of the contacts for Van der Pauw measurements, electron beam evaporation of Ti (3 nm) and thermal evaporation of Au (50 nm) was performed in the same vacuum chamber and conditions as previous Au UTMF deposition. The Ti and Au deposition rates in this case are 0.5 and 2 Å/s, respectively, also *in situ* measured by a quartz crystal microbalance.

UTMF Patterning. Au UTMFs with cloverleaf shape for Van der Pauw sheet resistance (Rs) measurements were fabricated via a standard lift-off process using S1805 photoresist on HMDS-primed high purity fused silica (HPFS) substrates. After resist exposure with a Heidelberg Maskless Aligner 150 and development on MF319, 0.5 nm CuO-seeded Au UTMFs of different thicknesses were deposited on the patterned substrate and then lifted-off in acetone. The same procedure was followed for the electrical contact patterns.

The Au nanodisk arrays were fabricated via nano imprinting lithography followed by a lift-off process. Prepatterned PDMS (polydimethylsiloxane) stamps were used to nanostructure the PMMA layer on top of the HPFS substrates. A 4% in weight PMMA (SIGMA Aldrich 200336 Poly(methyl methacrylate), average Mw ∼ 15 000 by GPC, powder) in toluene (labkem TOLN-G0P-1K0 Toluene GLR) is prepared and filtered using nylon syringe filters (Branchia SFNY-222−100 Nylon syringe filters, Pore: 0.22 μm) to avoid asteroids during the spin coating process. The PMMA is spin coated at 3000 rpm to obtain a layer thickness of 150 nm. The prepatterned PDMS stamp is composed of an array of pillars with 100 nm diameter, a periodicity of 200 nm, and a maximum height around 150 nm. The nanoimprinting process is performed using a CNI NIL tool at temperature of 140 °C above the PMMA glass transition and applying a pressure of 2 bar while heating and cool down to room temperature.[21] Once the sample is cooled down, the PDMS stamp is removed from the PMMA, leaving an array of holes on the PMMA with a thin residual layer. The prepatterned PMMA on HPFS substrates are first exposed to an Ar and O_2 plasma (40 sccm for both) and 10 W power in a reactive ion etching system (Oxford Plasmalab System 100) for 5 min to ensure there are no PMMA residues on the bottom of the patterned holes. Then, 0.5 nm CuO-seeded 4 nm Au UTMFs were deposited and the Au-coated PMMA was lifted-off in acetone.

Electrical, Optical, Morphological, and Chemical of UTMFs. The sheet electrical resistance (R_S) of the films were measured using cloverleaf shaped UTMFs with 2 nm Ti + 50 nm Au metal contacts in

https://doi.org/10.1021/acsami.2c22149
ACS Appl. Mater. Interfaces 2023, 15, 16204−16210

Van der Pauw configuration and a SMU Keysight B2901. The IR reflection spectra for tunable planar mirror based on Au UTMF were obtained with a Fourier-transform infrared spectrometer equipped with an IR microscope (Bruker Tensor II + Hyperion 2000). For the nanodisk shaped Au UTMFs on fused silica, morphology images were obtained using a scanning electron microscope Quanta 200 and transmittance spectra in the UV, Vis, and NIR wavelength ranges were measured using a Perkin Elmer LAMBDA 950 spectrometer. Chemical characterization (XPS) was performed with a with a SPECS PHOIBOS 150 hemispherical energy analyzer. The XPS data were used as measured with the C(1s) peak falling at 284.2 eV.

Simulation and Drude fit of UTMF IR Spectra. UTMFs IR R spectra in Figure 3d were simulated using a Python code implementing the transfer matrix method (TMM, Python TMM package developed by Byrnes[22]). For the UTMFs, a Drude permittivity $\varepsilon = 1 - 1/\left(\frac{\omega^2}{\omega_p^2} - i\varepsilon_0\rho\omega\right)$ was assumed, where ω_p is the plasma frequency and $\rho = 1/(\varepsilon_0\,\omega_p^2\tau)$ is the electrical resistivity.[3] To compute the R spectrum as a function of the UTMF thickness t, ω_p was fixed while ρ (or equivalently τ) was obtained from experimental values of sheet resistance R_S as $\rho = R_s t$, where t is the UTMF thickness interpolated from the 0.5 nm CuO-seeded Au UTMF percolation curve.[6] For fused silica substrate, the permittivity from Kitamura[20] was used.

Photoreduction Experiments. Sample surface oxidation has been performed by exposing to an O_2 plasma with an oxygen flow of 200 mL/min and power of 150 W for 3 min, in a plasma asher (Tepla 300). For the photoreduction experiments UTMF sheet resistance was measured under mounted Thorlabs LEDs irradiation and inside a climate chamber (Vötsch VCL 7003) in order to control the temperature and humidity conditions. Photoreduction of UTMFs for XPS measurements and wavelength dependence experiments has been performed with direct LED illumination with a distance between the light source and the sample of about 1 cm. For the rest of experiment a Newport M-20X with 0.4 numerical aperture was mounted on the LEDs to focalize the beam onto the sample. Irradiance values for all the cases has been measured with a Thorlabs PDA10A-EC Si amplified detector.

■ ASSOCIATED CONTENT

Supporting Information

The Supporting Information is available free of charge at https://pubs.acs.org/doi/10.1021/acsami.2c22149.

XPS spectrum of the O(1s) band of a 3 nm Au UTMF after O_2 plasma, AuO_x reduction evolution without light irradiation (PDF)

■ AUTHOR INFORMATION

Corresponding Authors

Daniel Martínez-Cercós − *ICFO-Institut de Ciencies Fotoniques, The Institute of Photonic Sciences, Barcelona 08860, Spain;* orcid.org/0000-0002-1514-0191; Email: daniel.martinez@icfo.eu

Valerio Pruneri − *ICFO-Institut de Ciencies Fotoniques, The Institute of Photonic Sciences, Barcelona 08860, Spain; ICREA-Institució Catalana de Recerca i Estudis Avançats, Barcelona 08010, Spain*; Email: valerio.pruneri@icfo.eu

Authors

Bruno Paulillo − *ICFO-Institut de Ciencies Fotoniques, The Institute of Photonic Sciences, Barcelona 08860, Spain;* orcid.org/0000-0002-6675-0141

Jessica Barrantes − *ICFO-Institut de Ciencies Fotoniques, The Institute of Photonic Sciences, Barcelona 08860, Spain*

Jose Mendoza-Carreño − *Institute of Materials Science of Barcelona ICMAB-CSIC Campus UAB, Bellaterra 08193, Spain*

Agustín Mihi − *Institute of Materials Science of Barcelona ICMAB-CSIC Campus UAB, Bellaterra 08193, Spain;* orcid.org/0000-0003-3821-7881

Todd St. Clair − *Corning Research and Development Corporation, Corning, New York 14831, United States*

Prantik Mazumder − *Corning Research and Development Corporation, Corning, New York 14831, United States*

Complete contact information is available at: https://pubs.acs.org/10.1021/acsami.2c22149

Author Contributions

The manuscript was written through contributions of all authors. All authors have given approval to the final version of the manuscript.

Notes

The authors declare no competing financial interest.

■ ACKNOWLEDGMENTS

This work was partially funded by CEX2019-000910-S [MCIN/AEI/10.13039/501100011033], and the project TUNA-SURF (PID2019-106892RB-I00) from Fundació Cellex, Fundació Mir-Puig, and Generalitat de Catalunya through CERCA and Agència de Gestió d'Ajuts Universitaris i de Recerca (2021 SGR 01458). This project received funding from the European Unio's Horizon 2020 Research and Innovation Programme under Marie Skłodowska-Curie grant agreement No. 754510, and from Ayuda (PRE2017-082781) funded by MCIN/AEI/10.13039/501100011033 y FSE "El FSE invierte en tu futuro". This project received funding from the Spanish Ministerio de Ciencia e Innovación through grant PID2019-106860GB-I00/AEI/10.13039/501100011033 and FUNFUTURE (CEX2019-000917-S, Spanish Severo Ochoa Centre of Excellence program). J.M.C. acknowledges FPI fellowships (PRE2020-09411) from MICINN cofinanced by the European Social Fund and the Ph.D. program in Materials Science from Universitat Autònoma de Barcelona.

■ REFERENCES

(1) Maniyara, R. A.; Mkhitaryan, V. K.; Chen, T. L.; Ghosh, D. S.; Pruneri, V. An Antireflection Transparent Conductor with Ultralow Optical Loss (<2%) and Electrical Resistance (<6 Ω Sq-1). *Nat. Commun.* **2016**, *7* (1), 13771.

(2) Ji, C.; Liu, D.; Zhang, C.; Jay Guo, L. Ultrathin-Metal-Film-Based Transparent Electrodes with Relative Transmittance Surpassing 100%. *Nat. Commun.* **2020**, *11* (1), 3367.

(3) Luhmann, N.; Høj, D.; Piller, M.; Kähler, H.; Chien, M. H.; West, R. G.; Andersen, U. L.; Schmid, S. Ultrathin 2nm Gold as Impedance-Matched Absorber for Infrared Light. *Nat. Commun.* **2020**, *11*, 2161.

(4) Maniyara, R. A.; Rodrigo, D.; Yu, R.; Canet-Ferrer, J.; Ghosh, D. S.; Yongsunthon, R.; Baker, D. E.; Rezikyan, A.; García de Abajo, F. J.; Pruneri, V. Tunable Plasmons in Ultrathin Metal Films. *Nat. Photonics* **2019**, *13* (5), 328−333.

(5) Manjavacas, A.; García de Abajo, F. J. Tunable Plasmons in Atomically Thin Gold Nanodisks. *Nat. Commun.* **2014**, *5*, 3548.

(6) Martínez-Cercós, D.; Paulillo, B.; Maniyara, R. A.; Rezikyan, A.; Bhattacharyya, I.; Mazumder, P.; Pruneri, V. Ultrathin Metals on a Transparent Seed and Application to Infrared Reflectors. *ACS Appl. Mater. Interfaces* **2021**, *13* (39), 46990−46997.

(7) Petach, T. A.; Lee, M.; Davis, R. C.; Mehta, A.; Goldhaber-Gordon, D. Mechanism for the Large Conductance Modulation in

Electrolyte-Gated Thin Gold Films. *Phys. Rev. B - Condens. Matter Mater. Phys.* **2014**, *90* (8), 1−5.
(8) Irissou, E.; Denis, M. C.; Chaker, M.; Guay, D. Gold Oxide Thin Film Grown by Pulsed Laser Deposition in an O2 atm. *Thin Solid Films* **2005**, *472* (1−2), 49−57.
(9) Machalett, F.; Edinger, K.; Melngailis, J.; Diegel, M.; Steenbeck, K.; Steinbeiss, E. Direct Patterning of Gold Oxide Thin Films by Focused Ion-Beam Irradiation. *Appl. Phys. A Mater. Sci. Process.* **2000**, *71* (3), 331−335.
(10) King, D. E. Oxidation of Gold by Ultraviolet Light and Ozone at 25 °C. *J. Vac. Sci. Technol. A Vacuum, Surfaces, Film.* **1995**, *13* (3), 1247−1253.
(11) Stadnichenko, A. I.; Koshcheev, S. V.; Boronin, A. I. Oxidation of the Polycrystalline Gold Foil Surface and XPS Study of Oxygen States in Oxide Layers. *Moscow Univ. Chem. Bull.* **2007**, *62* (6), 343−349.
(12) Higo, M.; Matsubara, Y.; Kobayashi, Y.; Mitsushio, M.; Yoshidome, T.; Nakatake, S. Formation and Decomposition of Gold Oxides Prepared by an Oxygen-Dc Glow Discharge from Gold Films and Studied by X-Ray Photoelectron Spectroscopy. *Thin Solid Films* **2020**, *699* (\), 137870.
(13) Tanaka, K. I.; Tamaru, K. A General Rule in Chemisorption of Gases on Metals. *J. Catal.* **1963**, *2* (5), 366−370.
(14) Ono, L. K.; Roldan Cuenya, B. Formation and Thermal Stability of Au2O3 on Gold Nanoparticles: Size and Support Effects. *J. Phys. Chem. C* **2008**, *112* (12), 4676−4686.
(15) De Anda Villa, M.; Gaudin, J.; Amans, D.; Boudjada, F.; Bozek, J.; Evaristo Grisenti, R.; Lamour, E.; Laurens, G.; Macé, S.; Nicolas, C.; Papagiannouli, I.; Patanen, M.; Prigent, C.; Robert, E.; Steydli, S.; Trassinelli, M.; Vernhet, D.; Lévy, A. Assessing the Surface Oxidation State of Free-Standing Gold Nanoparticles Produced by Laser Ablation. *Langmuir* **2019**, *35* (36), 11859−11871.
(16) Tsai, H.; Hu, E.; Perng, K.; Chen, M.; Wu, J. C.; Chang, Y. S. Instability of Gold Oxide Au2O3. *Surf. Sci.* **2003**, *537* (1−3), L447.
(17) Vincent Crist, B. *Handbook of Monochromatic XPS Spectra*; Wiley, 2000.
(18) Takamatsu, T.; Uehara, K.; Sasaki, Y.; Miyahara, H.; Matsumura, Y.; Iwasawa, A.; Ito, N.; Azuma, T.; Kohno, M.; Okino, A. Investigation of Reactive Species Using Various Gas Plasmas. *RSC Adv.* **2014**, *4* (75), 39901−39905.
(19) Fleisch, T. H.; Zajac, G. W.; Schreiner, J. O.; Mains, G. J. An XPS Study of the UV Photoreduction of Transition and Noble Metal Oxides. *Appl. Surf. Sci.* **1986**, *26* (4), 488−497.
(20) Kitamura, R.; Pilon, L.; Jonasz, M. Optical Constants of Silica Glass from Extreme Ultraviolet to Far Infrared at near Room Temperature. *Appl. Opt.* **2007**, *46* (33), 8118.
(21) Dore, C.; Osmond, J.; Mihi, A. A Water-Processable Cellulose-Based Resist for Advanced Nanofabrication. *Nanoscale* **2018**, *10* (37), 17884−17892.
(22) Byrnes, S. J. Multilayer Optical Calculations. *arXiv Prepr.* **2016**, arXiv1603.02720.

https://doi.org/10.1021/acsami.2c22149
ACS Appl. Mater. Interfaces 2023, 15, 16204−16210